

A COMPARATIVE STUDY OF THREE PORE-SCALE RECONSTRUCTION AND PORE-NETWORK EXTRACTION TECHNIQUES

Arjen Cense and Fons Marcelis
Shell International Exploration & Production, Rijswijk, the Netherlands

This paper was prepared for presentation at the International Symposium of the Society of Core Analysts held in Abu Dhabi, UAE 29 October-2 November, 2008

ABSTRACT

We present the results of a comparative study of three third party pore-scale reconstruction techniques and their pore-network extraction techniques, applied to a clay-rich sandstone reservoir. With each technique one 3D model of the rock was constructed on the basis of a micro-CT or a backscattered scanning electron microscopy image. Subsequently, a pore-network model was extracted from the 3D model. Although each pore-scale reconstruction and pore-network extraction technique is different, they should give similar results for single phase and multi-phase flow properties when applied on the same rock.

We determined porosity and absolute permeability values for each of the 3D models by means of Lattice-Boltzmann simulations and the results were compared against laboratory measurements. Primary drainage relative permeability and capillary pressure were determined using a multi-phase flow simulation on the pore-network model of the 3D rock model, and these were compared against laboratory experiments. Porosity was matched within 10%, while the absolute permeability of the 3D model was matched with laboratory measurements for two out of three methods. The quality of the networks was tested by simulating first drainage capillary pressure and relative permeability, and although not all multi-phase parameters are predicted well, the results are promising.

INTRODUCTION

To predict the performance of a reservoir, in particular when multiple phases are involved (water, gas, oil), one needs saturation dependent properties such as relative permeability and capillary pressure. In general, these properties are experimentally determined by flooding water and oil through small sized (4 cm × Ø 2.8 cm) rock samples taken from a core of the reservoir. The procedure is rather time consuming and expensive, since it involves cleaning, standard core analysis (determination of porosity and brine permeability), ageing (restoration of the wettability) and finally, special core analysis experiments (determination of capillary pressure and relative permeability). The whole procedure easily exceeds three months. Pore network modeling may potentially add significant value, as it can extend a small experimental dataset on the basis of 2D or 3D images on a much shorter timescale. If successful, it makes it easier to study the sensitivity of parameters such as porosity, permeability and wettability (clay content) on relative permeability and capillary pressure. Furthermore, it helps in understanding fundamental

flow processes at the microscopic level and ultimately in quantifying these microscopic effects on a macroscopic (core plug) level.

The concept of pore network modeling is depicted in Figure 1. A 3D model of the pore space can be obtained using X-ray microcomputed tomography (Arns et al., 2005), using process-based methods (Bakke and Øren, 1997) or using statistical methods (Okabe and Blunt, 2004; Wu et al., 2006) (Fig. 1 (a)).

Porosity is calculated from the ratio of ‘void’ voxels¹ and total voxels, as long as a proper threshold between void and matrix is chosen. The absolute (single phase) permeability is calculated using Lattice Boltzmann simulations (Jin et al., 2004) on the voxelized binary image.

Saturation dependent properties, such as relative permeability and capillary pressure, can in principle be calculated by solving the Navier-Stokes equation (Adler et al., 1990) or by performing Lattice-Boltzmann simulations (Keehm and Mukerji, 2004) directly on the 3D pore space. Although these numerical methods give very accurate results on fluid flow in complex porous media, they are computationally very demanding, and model sizes are often not large enough to capture a representative elementary volume (REV) (Keehm and Mukerji, 2004). A REV is the minimum volume above which a measured quantity on the network does not significantly change. It was demonstrated by Keehm and Mukerji (2004) that for permeability, the REV should be larger than 10 autocorrelation lengths, and that for relative permeability the REV should be larger than 20 autocorrelation lengths. The autocorrelation length, a , or two-point correlation function length, is a characteristic length scale of the porous rock. It gives the correlation of the structural elements representing the pore space and can therefore be used to compare 3D models with the reservoir rock. Let $I(\mathbf{x})$ be an indicator function that has the following properties

$$I(\mathbf{x}) = \begin{cases} 1, & \mathbf{x} \in \text{pore space} \\ 0, & \mathbf{x} \in \text{matrix} \end{cases} \quad (1)$$

The statistical average of I represents the porosity, $\varphi = \langle \sum_i I(\mathbf{x}_i) \rangle$, where angular brackets denote volumetric averaging. The two-point correlation function $C_2(\mathbf{u})$ is defined as

$$C_2(\mathbf{u}) = \frac{\langle (I(\mathbf{x}) - \varphi) \cdot (I(\mathbf{x} + \mathbf{u}) - \varphi) \rangle}{\varphi(1 - \varphi)}, \quad (2)$$

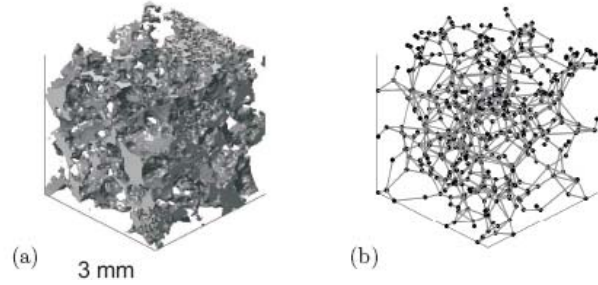


Figure 1: (a) 3D image of a sandstone along with (b) a topologically equivalent network representation.

¹ A voxel is a 3D representation of a pixel, having a width, length and depth equal to the image resolution

and gives the probability of finding two end points of a ‘ruler’ with length \mathbf{u} within the same phase. Apart from the fact that the model needs to be large enough in size, we do not want to lose too much detail of the pore structure by coarsening the voxels. Keehm and Mukerji (2004) showed that the error made in absolute permeability and relative permeability remains reasonably small when the grid spacing d is smaller than $d \leq a/10$. Here, a is the correlation length which can be calculated from fitting the two-point correlation function with an exponential function $M(\mathbf{u})$ (Keehm and Mukerji, 2004):

$$M(\mathbf{u}) = (\varphi - \varphi^2) \exp\left[-\frac{3\mathbf{u}}{a}\right] + \varphi^2. \quad (3)$$

Larger models can be simulated if the pore space is simplified by representing pore bodies as ‘balls’ and pore constrictions – or pore throats – as ‘tubes’, see Fig. 1 (b). Both ‘balls’ and ‘tubes’ can have an angular shape, allowing the presence of oil and water to be modeled in a realistic manner. The resulting ‘pore network model’ can be solved for capillary pressure and relative permeability by applying certain rules for pore filling events (Øren et al., 1998). It is assumed that the flow is dominated by capillary forces, meaning that viscous forces are insignificant. The capillary number N_c , should then be smaller than 10^{-5} ,

$$N_c = \frac{\mu u}{\sigma} < 10^{-5}, \quad (4)$$

where μ is the dynamic viscosity in Pa s, u is the Darcy flow velocity in m/s and σ is the interfacial tension in N/m. This condition is generally met in actual reservoir water floods.

In many cases, new concepts of pore-scale reconstruction techniques are tested either on artificial systems, such as bead packs, or on clean sandstones such as Fontainebleau or Bentheim. Most (sandstone) reservoir rocks however show different minerals and often contents of clay. The purpose of this communication is to test three pore-scale reconstruction methodologies on a clay-rich sandstone and make a comparison of the simulated rock properties with experimental results.

MATERIALS AND METHODS

Three third party pore-scale reconstruction techniques were tested on a clay-rich sandstone: micro-CT, so called pore architecture models (PAMs) and process based reconstruction. The core plugs came from two locations ‘1’ and ‘3’, 40 ft apart, but core properties were almost similar in terms of porosity and permeability. Multiple (twin) plugs were drilled at each location. Two plugs were used in laboratory experiments (index ‘A’ and ‘B’), and trim ends were used for thin section imaging and for Backscattered Scanning Electro Microscopy imaging (BSEM). To capture a large enough image with high enough resolution, 4×4 mosaic BSEM images were taken, see Figure 2. A twin plug from location ‘3’ was provided to the micro-CT third party, the BSEM image from location ‘3’ was provided to the process-based reconstruction third party and a BSEM image from location ‘1’ was provided to the PAMs third party.

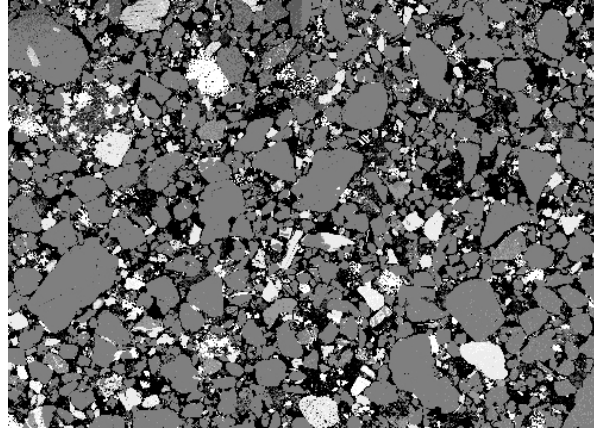


Figure 2: BSEM image of sandstone rock from position ‘1’. Actual width of the image is approximately 4 mm.

Each third party provided a 3D reconstructed (voxelized) model of the rock as well as a network model that was made using their own network extraction algorithms. We calculated absolute permeability and two-point correlation function of the 3D voxelized models using the same software (Numerical Rocks, Trondheim, Norway) so that the quality of the pore scale reconstruction technique itself could be analyzed. We used the statistical properties of the BSEM images and results from the laboratory experiments as a benchmark. In addition, we calculated certain properties of the network models (absolute permeability, first drainage capillary pressure and first drainage water relative permeability) using the same pore network simulator (PoreSim, Numerical Rocks, Trondheim, Norway) and compared these with results from laboratory experiments.

Laboratory experiments

Samples were drilled from a sandstone reservoir core using reservoir brine. Homogeneity of the samples was checked beforehand by taking CT-scans of the core. The samples were cleaned using cycles of toluene, azeotropic mixture of chloroform, methanol and water, and subsequently dried in a vacuum oven at 95 °C. Standard core analysis was performed to obtain porosity and brine permeability, see Table 1. Viscosity and density of the reservoir crude and brine were measured at 20 °C and 70 °C, which were the temperatures at which laboratory experiments were carried out.

Vacuum brine-filled samples were desaturated with dead crude to initial water saturation using an automated centrifuge (Beckman, L8-60M/P Ultracentrifuge) in multi-speed mode, providing drainage oil/water capillary pressure curves as well as the water relative permeability (Hassler and Brunner, 1945; Hagoort, 1980). In addition, the experiments were matched with numerical simulations using Shell’s in-house reservoir simulator (MoReS).

Table 1: Basic core properties

sample #	porosity (-)	permeability (mD)
1A	0.242	140
1B	0.242	162
3A	0.242	139
3B	0.242	149

Mercury-air drainage capillary pressure curves were determined on end pieces of the samples.

BSEM images were obtained from polished and impregnated core plug end-pieces, see Figure 2. We determined the autocorrelation function and the porosity from these images. In addition, we measured clay content of the samples from image analysis of the BSEM images, from point counting of thin section images and from XRD (X-Ray Diffraction) analysis. This gave clay contents of 11.8%, 13.7% and 7.8% for sample #1 and 9.8%, 18.3% and 8.0% for sample #3. The point-counting data had only 100 points and was less reliable. A clay content of 10% for both samples seems to be appropriate.

The following sections describe the concept of three third-party methodologies that were used to model the 3D pore space.

X-Ray microcomputed tomography (micro-CT)

X-Ray tomography is used by Australian National University (ANU, Canberra, Australia) to make 3D images of an object on the basis of differences in attenuation of the X-ray radiation. Images are obtained using a high-resolution (2 μm) and large-field X-ray μCT set-up (Sakellariou et al., 2003). The CT scanner has a cone beam geometry, which means that the resolution is limited by the size of the X-ray source, which is around 2 μm . Images are captured using a 16 bit X-ray detector, 2048 \times 2048 pixels in size. Tomograms are acquired using filtered Brehmsstrahlung² with the X-ray source set to a voltage of 80 kV and a current of 200 μA .

One 'image' of the sample gives the linear attenuation along the line of sight between the source and the detector. To obtain a 3D image, the sample is rotated 360° in steps. The 3D image is obtained by deconvolution of the raw images. This gives the linear attenuation of each voxel. In order to discriminate between minerals (clay, quartz, carbonate), it is necessary to apply a series of filters (Sheppard et al., 2004). Networks were extracted using the algorithms as described in Sheppard et al. (2005). These steps are illustrated in Figure 3.

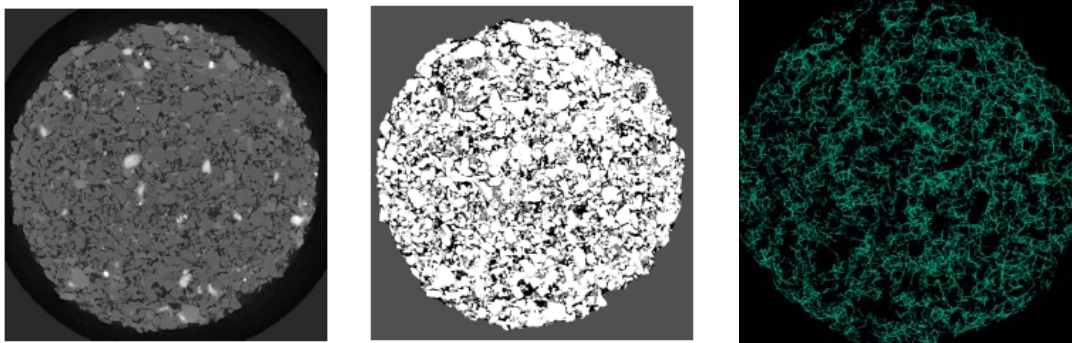


Figure 3: From left to right: 2D filtered $\mu\text{-CT}$ image slice, segmented image and pore network model.

² Brehmsstrahlung is continuous X-ray radiation that originates when electrons are decelerated in the electric field of a nucleus.

Pore Architecture Modeling

Pore Architecture Modeling is a reconstruction method developed by Heriot-Watt University (Edinburgh, United Kingdom) that creates 3D models of porous rock from 2D thin-section images, and subsequently extracts from these models the complete geometry/topology of the pore network, see Figure 4.

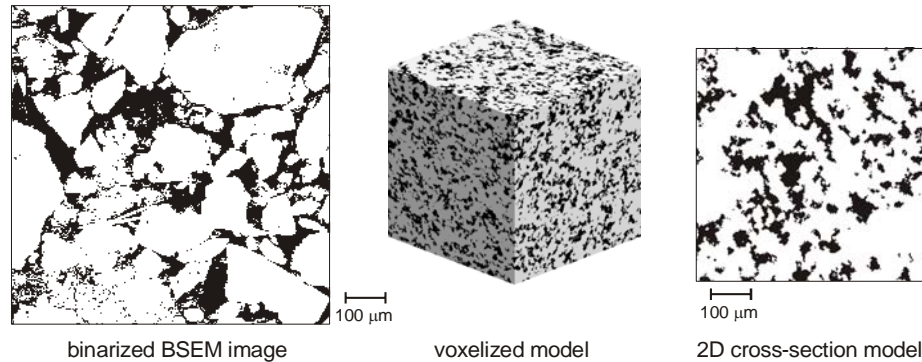


Figure 4: PAMs applied on binary form of BSEM image.

The method uses Markov Chain Monte Carlo (MCMC) simulation. It considers spatial structure information (derived from 2D thin section data in the x, y and z planes) that identifies all the transition probabilities between the voids and solids of the medium for a given local training lattice stencil. The input data is taken from image analysis, but the approach differs in one very important respect from published two-point (or multipoint) correlation methods (see e.g. Okabe and Blunt, 2004). The method involves a complicated multiple-voxel interaction scheme (a high-order neighbourhood system) to generate individual realisations that have structure characteristics matching the input data (Wu et al., 2006). It is a non-iterative single-scan method, which is very efficient compared with traditional multi-point statistics methods. This MCMC reconstruction approach and the models it generates are referred to as ‘pore architecture models’, or PAMs. Networks were extracted using the approach from Jiang et al. (2007).

Process Based Reconstruction

Process based reconstruction is a technique developed by Numerical Rocks (Trondheim, Norway; Bakke and Øren, 1997). It explicitly mimics the rock forming processes sedimentation, compaction and diagenesis. Sedimentation is modeled by depositing spherical or ellipsoidal grains into the model box at random position or at global minimum energy positions. Compaction (e.g. due to overburden pressure) is modeled by grain relocation in a specified direction. Various diagenetic processes are modeled, such as cementation by quartz or carbonates, clay formation and feldspar dissolution. Input parameters to the modeling algorithms are extracted from quantitative and qualitative analysis of BSEM images and/or integration of other data (e.g. X-ray diffraction, point counting). Note that geological processes are not modeled in time, but that the resulting model is a realistic representation of the final result of these processes, see Figure 5. Networks were extracted using the method of Bakke and Øren (1997).

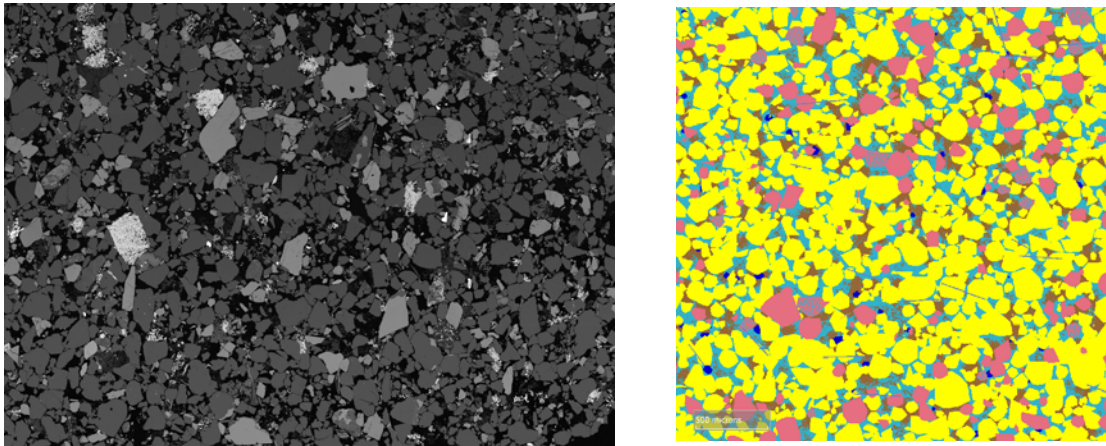


Figure 5: BSEM image of sample from location ‘3’ (left). Result of process based reconstruction (right). Quartz grains are yellow, feldspar grains are pink, clay is brown and pore space is light blue.

RESULTS

The results of the three pore scale reconstruction methodologies are depicted in Figures 6-9. In contrast to PAMs, the micro-CT method and process-based method take into account the abundance of clay in the reconstruction step. This is important to account for microporosity in the clay and thus to enable modeling clay bound water. The properties of the 3D voxelized models are summarized in Table 2.

Table 2: Properties of the voxelized 3D models.

method	imaged from #	size (# voxels)	resolution (μm)	clay (%)	porosity (-)	permeability (mD)
micro-CT	3	400 ³	2.8	15	0.27 ³	455
PAMs	1	500 ³	4	N/A	0.26	122
process based	1	1000 ³	3	10.5	0.23 ³	218

Porosity and permeability of the voxelized image

The micro-CT model overestimates the permeability by a factor of 3. The other two methods give absolute permeabilities within 20% (PAMs) and 40% (process based). The porosity measured on the BSEM image was used as input for the process based method and for the PAMs method and should be close to the experimentally measured value. Due to small scale heterogeneities 2D porosity values may differ from 3D porosities.

Clay content

Both samples showed 10% of clay abundance. The μ -CT data overestimated the clay content with 5% at 15%; PAMs did not consider clays explicitly. The process based reconstruction model had 10.5% of clay.

³ includes 50% microporosity

Two point correlation function

The two-point correlation function was calculated on the BSEM image and compared to the two-point correlation function on the 3D models. For the latter, we calculated the averaged two-point correlation function of the x -, y - and z direction. For the micro-CT and process based reconstruction technique the agreement is quite good, see Figure 6.

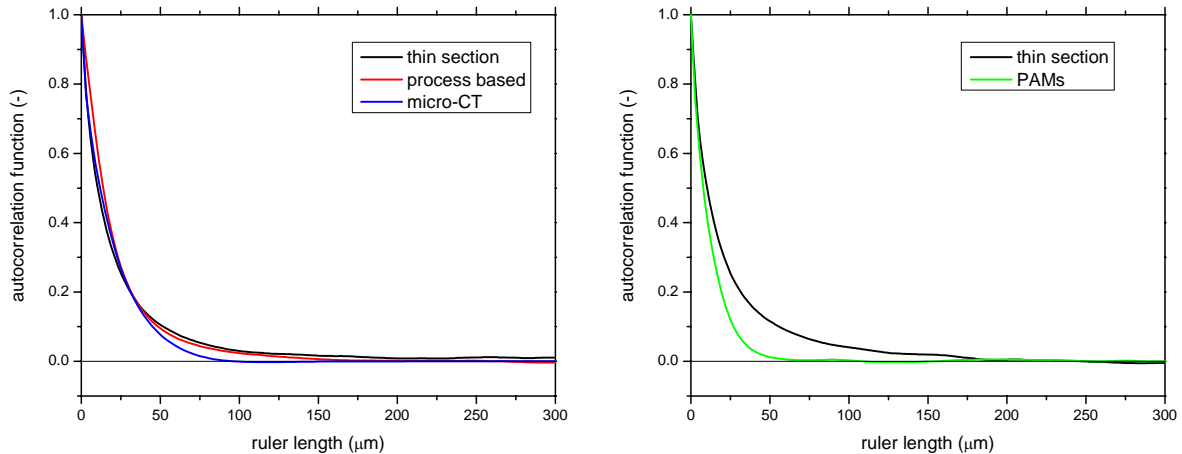


Figure 6: Autocorrelation functions for micro-CT reconstruction and process based reconstruction (left) and for PAMs (right) compared to that from BSEM image.

For the PAMs, the agreement is poor (Figure 8). For the first two, the autocorrelation length is 100 μm and for the latter it is 50 μm , indicating that for accurate absolute permeability calculations, model sizes of at least 1000 μm and 500 μm are needed. This condition is met for all techniques. To be able to make accurate *relative* permeability simulations, the models should be at least twice as large (Keehm and Mukerji, 2004), a condition that is not met in all cases.

Network permeability

Networks were in all cases extracted from the voxelized images by the third parties themselves, see Table 3 for the network properties. The average number of pore throats that are connected to each pore body is called the coordination number or connection number. It is an important number as it influences the behaviour of network models significantly.

Table 3: Properties of the pore networks

method	# pores	# throats	coordination number (mean/max)	porosity (-)	permeability (mD)
micro-CT	53 942	103 529	3.8/57	0.23 ³	261
PAMs	311 122	421 648	2.70/25	0.26	107
process based	154 951	296 922	3.89/19	0.23	44.6

The network from μ -CT and process based reconstruction give a similar coordination number (3.8 and 3.9) which is much higher than the 2.7 from PAMs. Network porosity and network absolute permeability were determined using the same pore network simulator (PoreSim, Numerical Rocks, Trondheim). Absolute permeability of the network model should closely match the absolute permeability of the 3D model. The micro-CT and PAMs matched the permeability within a factor of 1.7 and 1.1 respectively. The process-based model overestimated the absolute permeability of the 3D model with a factor of 4.8⁴.

First drainage capillary pressure and relative permeability

Primary drainage capillary pressure, P_c , and relative permeability, k_r , was obtained from calculations on the networks. For details of the pore network simulator that was used for all flow simulations, the reader is referred to Bakke and Øren (1997).

PAMs and the process-based reconstruction methods provide network models that show similar behavior, see Figure 7 and Figure 9. The entry pressure, i.e. the pressure at which oil first enters the system is matched within 200 Pa. This number is important for determining the oil-water contact from pressure measurements in the borehole (which give the free water level at which $P_c = 0$). The micro CT method underestimates the entry pressure slightly with 500 Pa, see Figure 7. All curves show a flatter plateau region compared to the experimental P_c , indicating that the pore network has either less connectivity than the rock, or that the distribution of pore throat radii is narrower in the network. The connate water saturation, S_{wc} , is closely connected to the abundance of clay.

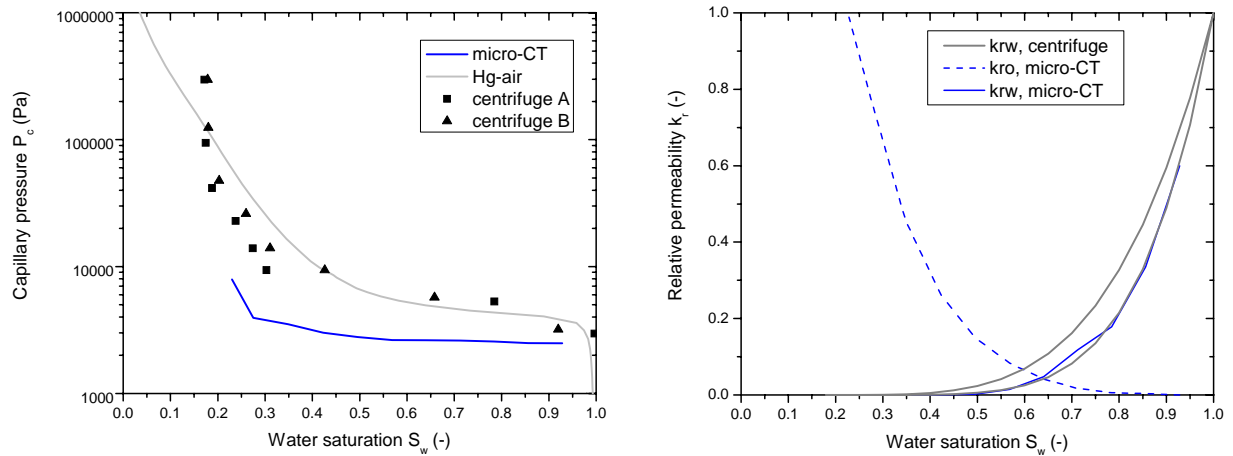


Figure 7: Primary drainage (oil-water) capillary pressure (left) and relative permeability (right) as function of water saturation for micro-CT network simulations. For capillary pressure, simulations are compared against normalized mercury-air data and oil-water centrifuge data on twin plugs. Relative permeability simulations are compared against oil-water centrifuge data.

⁴ For other models made using process based reconstruction on the same sandstone (not shown here), the differences between voxelized and network permeability were less, but considerable.

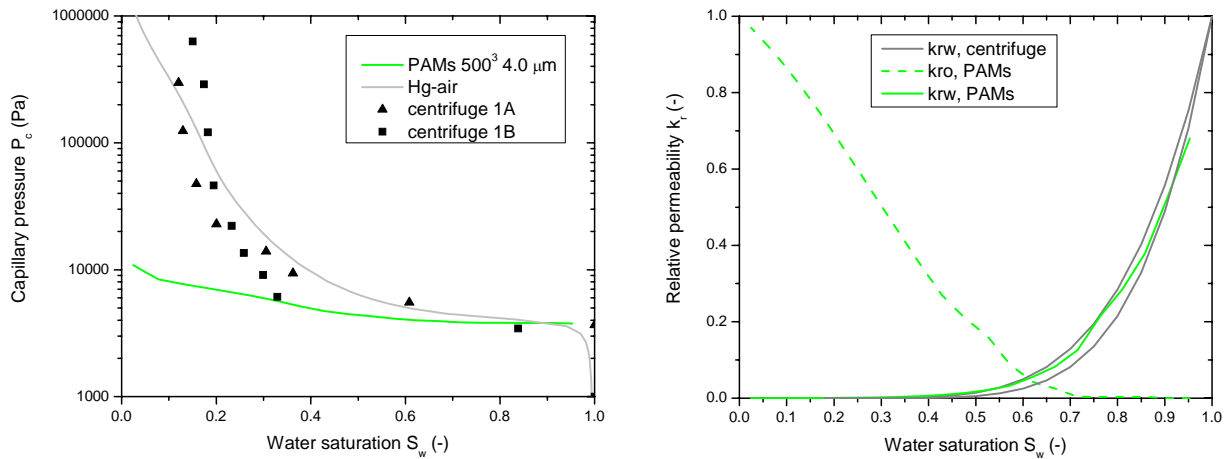


Figure 8: Primary drainage (oil-water) capillary pressure (left) and relative permeability (right) as function of water saturation for PAMS network simulations.

For the micro CT a clay microporosity of 50% was assumed and we obtained $S_{wc} = 0.23$. For the process based model $S_{wc} = 0.17$, which agrees with the experiment for which $S_{wc} = 0.17$. For PAMs, S_{wc} is virtually equal to zero. This difference is caused by the ways clays are treated. In PAMs, clays are regarded as part of the matrix, whereas in process based reconstruction and micro-CT, clay is modeled as a separate phase and clay-bound water is modeled explicitly.

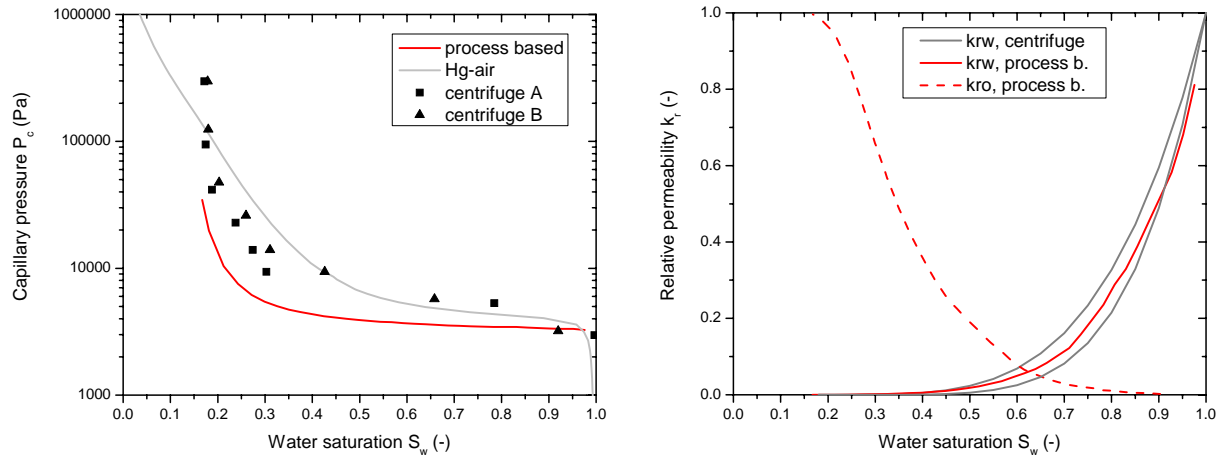


Figure 9: Primary drainage (oil-water) capillary pressure (left) and relative permeability (right) as function of water saturation for process based network simulations.

The maximum P_c that can be obtained from a network model is related to the resolution d , and it is estimated using

$$P_{c,\max} = \frac{4\sigma \cos\theta}{d}, \quad (5)$$

which is valid for purely cylindrical tubes. Here, θ is the contact angle, which was between 0-10 in the primary drainage simulations where the rock was assumed to be water-wet. The interfacial tension was measured at 12 mN/m. The experimental results indicate that this clay-rich sandstone rock has structures below the image resolution of 2-4 micrometers and therefore cannot be predicted per definition.

The comparison between simulation and experiment shows good agreement for the water relative permeability curve for micro-CT (Figure 7), PAMs (Figure 8) and process based reconstruction (Figure 9), despite a poor reconstruction of the shape of the capillary pressure curve.

DISCUSSION AND CONCLUSION

We have tested three pore-scale reconstruction methodologies, μ -CT, PAMs and process based reconstruction, on a clay-rich sandstone reservoir rock.

The μ -CT approach gave 3D voxelized models for which the porosity was slightly overestimated, assuming a clay microporosity of 50%. There was good agreement of the two-point correlation function. The absolute permeability was overestimated by a factor of three. The network permeability was within a factor of two compared to the voxelized permeability. The network model gave a good prediction of connate water saturation, however, the entry pressure and curve shape factor of the P_c curve were poorly predicted. The simulated water relative permeability curve was within the experimental error bars.

The PAMs method gave a poor match with the two-point correlation function. Remarkably, the porosity, permeability of the voxelized image and permeability of the network model are in good agreement with the experimental results. Primary drainage capillary pressure simulations on the network showed a good prediction of entry pressure, but there was a lack of agreement for the connate water saturation and for the shape of the P_c curve. First drainage relative permeability was matched well with experimental results.

The process-based reconstruction method gave a good match with the two-point correlation function, porosity and absolute permeability of the voxelized model. The network model permeability was more than a factor of 4 smaller than the permeability of the voxelized image. The primary drainage capillary pressure simulations matched in terms of entry pressure and connate water saturation, but lacked precision on the curve shape. The water relative permeability curve was matched within the error bar of the experimental results.

We have demonstrated that pore-scale reconstruction techniques applied to this clay-rich reservoir rock can be predictive in single-phase properties, but that it cannot predict all aspects related to (primary drainage) multi-phase properties. We want to stress that the conclusions drawn in this communication are based on observations for a specific rock sample, and should under no circumstances be generalized to other rock types.

ACKNOWLEDGEMENTS

The authors greatly acknowledge K. Wu and M.I.J. van Dijke from Heriot-Watt University, M.A. Knackstedt, A. Sheppard and H. Averdunk from ANU and A. Mock, L. Alberts, K. Bendiksen and P.E. Øren from Numerical Rocks for their contributions. We thank W.J. Looyestijn and P. Valvatne from Shell for helpful discussions.

REFERENCES

14. Adler, P.M. , Jacquin, C.G. and Quiblier, J.A. (1990). Flow in simulated porous media . *International Journal of Multiphase Flow*, **16**: 691-712.
1. Arns, C., Bauget, F., Ghouss, A., Sakellariou, A., Senden, T., Sheppard, A., Sok, R., Pinczewski, W., Kelly, J., and Knackstedt, M. (2005). Digital core laboratory: petrophysical analysis from 3d imaging of reservoir core fragments. *Petrophysics*, **46**:260–277.
2. Bakke, S. and Øren, P. (1997). 3-D pore-scale modelling of sandstones and flow simulations in the pore networks. *SPE*, 35479.
3. Bakke, S. and Øren, P. (2002). Process based reconstruction of sandstones and prediction of transport properties. *Transport in Porous Media*. **46**: 311-343.
4. Hagoort, J. (1980). Oil recovery by gravity drainage. *SPE*, 7424-PA.
5. Hassler, G.L. and Brunner, E. (1945). Measurement of capillary pressure in small core samples. *Trans. AIME*, **160**: 114-123.
6. Jiang, Z., Wu, K., Couples, G., van Dijke, M.I.J., Sorbie, K.S. and Ma, J. (2007). Efficient extraction of networks from 3D porous media, *Water Resour. Res.*, **43**, W12S03, doi:10.1029/2006WR005780.
7. Jin, G., Patzek, T.W., and Silin, D.B. (2004). Direct prediction of the absolute permeability of unconsolidated and consolidated reservoir rock, *SPE*, 90084.
8. Keehm, Y. and Mukerji, T. (2004). Permeability and relative permeability from digital rocks: Issues on grid resolution and representative elementary volume. *SEG Int'l Exposition and 74th Annual Meeting, Denver, Colorado*.
9. Okabe, H. and Blunt, M. (2004). *Geostatistics Banff 2004*, volume 14, chapter Quantitative geology and statistics, pages 763-768. Springer Netherlands.
10. Øren, P., Bakke, S. and Arntzen, O. (1997). Extending predictive capabilities to network models. *SPE*, 52052.
11. Sakellariou, A., Arns, C.H., Limaye, A. Senden, T.J., Sheppard, A.P., Sok, R.M., Pinczewski, W.V., Knackstedt, M.A., Berge, L. and Øren, P. (2003) μ -CT facility for imaging reservoir rocks at pore scales. *SEG expanded abstracts historical series*. 1664-1667.
12. Sheppard, A.P., Sok, R.M. and Averdunk, H. (2004). Techniques for image enhancement and segmentation of tomographic images of porous materials. *Physica A*, **339**, 145-151.
13. Sheppard, A.P., Sok, R.M. and Averdunk, H. (2005). Improved pore network extraction methods. *Proceedings of the SCA, Toronto, 2005*.
14. Wu, K., van Dijke, M., Couples, G., Jiang, Z., Ma, J., Sorbie, K., Crawford, J., Young, I., and Zhang, X. (2006). 3D stochastic modelling of heterogeneous porous media - applications to reservoir rocks. *Transport in Porous Media*, **65**:443-467.